Atomic-Scale Imaging and Quantification of Electrical Polarisation in Incommensurate Antiferroelectric Lanthanum-Doped Lead Zirconate Titanate

Ian MacLaren, Rafael Villaurrutia, Bernhard Schaffer, Lothar Houben, and Aimé Peláiz-Barranco*

Lanthanum doping of zirconium rich lead zirconate titanate gives rise to incommensurate, long-period antiferroelectric structures. The structure of two stacking sequences in this incommensurate phase is determined using quantitative analysis of high-resolution scanning transmission electron microscopy images, with the lead atom positions located with an exceptional precision of about 6 pm. This allows the estimation of local polarisation variations across the stacking units, and the polarisation varies in an approximately sinusoidal fashion along the stacking direction. The measured peak Pb atom displacements of about 28 pm and peak polarisation values of about 60 μC cm^{-2} match extremely well to reported values for the commensurate antiferroelectric $PbZrO_3$ phase.

1. Introduction

Ferroelectric materials are highly significant commercially and find wide applicability for their dielectric and piezoelectric properties. It has long been recognised that useful properties arise at the morphotropic phase boundary between tetragaonal and rhombohedral forms in lead zirconate titanate, and more recently it has been suggested that in general the most interesting properties arise in such systems around phase boundaries between different polarisation orderings.[1,2] One phase boundary which has been of interest for some while is the phase boundary between antiferroelectric and ferroelectric orderings in lead zirconate titanate, and these materials are interesting for high-strain actuators and explosive shock sensors, utilising the large cell distortion that results from the reversible stress or electric field induced antiferroelectric-ferroelectric transition in these compositions. These materials are also of fundamental scientific interest, since whilst it is clear that diffraction reveals the presence of an incommensurate phase,[3–10] which is probably antiferroelectric,[11] the details of the atomic structure of the antiferroelectric ordering are completely unknown.

It has been known for some time that the incommensurate phases in doped lead zirconate titanate ($Pb(Zr,Ti)O_3$, PZT) have a long period ordering along a [110] direction of the primitive cubic perovskite unit cell with a periodicity of 6–8 (110) spacings.[3,5–9] High-resolution transmission electron microscopy (HRTEM) investigations have also shown that the stacking of the structural units along this direction can be irregular, leading to the incommensurate average periodicity,[3,6] but atomic-position measurements have hitherto not been attempted and there is consequently no clear picture of the distribution of polarisation on the atomic scale. The lack of long range periodicity makes it impossible to attempt with any confidence a refinement of atomic positions based on broad beam diffraction techniques, although it is clear from X-ray, neutron and electron diffraction studies that this phase must be orthorhombic with a pseudotetragonal perovskite substructure.[4,10] For this reason, the only reliable way to gain quantitative information on atom site locations is to use atomic-resolution electron microscopy.

The recent development of aberration correction for electron optics has allowed the introduction of a new generation of electron microscopes with resolutions well below 1 Å. This has also made it possible to measure the locations of atomic columns in ideal conditions from HRTEM imaging with precisions in the picometre range,[12,13] especially using the negative spherical aberration (C_s) imaging technique.[14] The application of such techniques to a variety of materials promises to deliver a hitherto undreamed wealth of insights into their structure and functionality. Similarly huge strides have been made in high-resolution scanning transmission electron microscopy (HRSTEM), and instruments with aberration-corrected probe forming

Dr. I. MacLaren, Dr. R. Villaurrutia, Dr. B. Schaffer
SUPA, School of Physics and Astronomy
University of Glasgow
Glasgow G12 8QQ, UK
E-mail: ian.maclaren@glasgow.ac.uk
Dr. B. Schaffer
SuperSTEM Laboratory
STFC Daresbury Laboratories
Keckwick Lane, Warrington WA4 4AD, UK
Dr. L. Houben
Ernst Ruska-Centre for Microscopy and Spectroscopy with Electrons (ER-C)
Research Centre Jülich, 52425 Jülich, Germany
Dr. A. Peláiz-Barranco
Facultad de Física-Instituto de Ciencia y Tecnología de Materiales
Universidad de La Habana. San Lázaro y L
Vedado. La Habana 10400, Cuba

DOI: 10.1002/adfm.201101220

lenses exist with spot sizes <0.7 Å in diameter, allowing sub-Ångström-resolution in HRSTEM. HRSTEM using high angle annular dark field (HAADF) imaging has significant advantages over HRTEM in terms of the ease of interpretation of images; images consist of bright atoms on a dark background even at larger thicknesses of ⩾ 10 nm and there is no need for exit wave reconstruction; HRTEM, even using negative C_s imaging suffers from contrast reversals at very small thicknesses of just a few nanometres making sample preparation extremely challenging and makes beam-induced changes to domain structures extremely likely. Small displacements of atomic columns in perovskites are also visible and measurable in HAADF–HRSTEM images and have recently been used to study features such as polarisation changes at interfaces and polarisation rotation in ferroelectrics.[15–19] Unfortunately, any scanning system suffers from distortions, both arising from miscalibrations, hysteresis and nonlinearities in the scanning system, as well as from drift of the sample during scan acquisition, and the presence of such scan distortions places a limit on high-precision metrology of atom site locations in HRSTEM images, although some progress has been made on distortion correction of and quantitative structural refinement from HRSTEM images.[20–23] The present work applies distortion correction of HRSTEM images to provide picometre-resolution measurements of Pb column positions in incommensurate antiferroelectric La-doped lead zirconate titanate allowing us to make the first ever determination of the atomic structure of two different stacking sequences found in the incommensurate phase, as well as to make estimates of the local polarisation variation across these long period stacking sequences.

2. Results and Analysis

Figure 1a shows a HRSTEM image recorded with the bright-field detector from a single scan of an area suitably oriented with the [001] axis along the beam direction (shown on a false colour scale to enhance contrast for the reader); it is clear in this image that layered structures are present, with vertical layers in the lower left, and horizontal layers in the upper right, with a 90° domain boundary between. Figure 1b shows a single HAADF image recorded simultaneously with the image of Figure 1a (shown as a false colour image to enable the reader to better view the sometimes subtle contrast variations). As will be obvious to the reader, this image is very noisy and precision atom site location would be difficult and unreliable in this case. One frequently applied solution to this problem is to take a slow scan with a longer dwell time per pixel, but this has the weakness for quantitative position measurement that sample drift will distort the image to some degree – which may well be non-uniform from top to bottom. Our alternative solution to this problem was to repeatedly and rapidly scan the same area and then cross correlate and sum all the (in this case 26) images using a specially designed software tool[24] to produce the average image shown in Figure 1c; this image is much clearer and the atom site locations are much more easily identifiable, and drift should have had a minimal effect. The high atomic number Pb atoms scatter most strongly to high angles and are the brightest atoms in the image but weaker atom site positions may also be recognised in the centres of the squares as Zr/Ti columns; weakly scattering oxygen atoms are not visible in this image. It should be noted that the sample was thinnest at the top left and gets thicker towards the lower part, thus accounting for the increased brightness and higher background intensity in the lower part. All areas used in the following quantifications were chosen from thinner parts of the specimen in this image to avoid the effects of excessive beam spreading in the thicker parts of the specimen.

Figure 2a shows a plot of the peak positions determined by image analysis of a representative area of horizontal stripes: area 1 of Figure 1c; the unit cells for the repeating structure are indicated on this plot and a repeating pattern of lead ion displacements is already clearly recognisable, although some shear distortion of the scan is also obvious. This was then processed through a variety of stages (described in detail in the supplementary material) to remove scan distortions, all of which are based on the fact that the parameters of the perovskite subcell are already well known[4,25]: specifically, we expect the cell to be

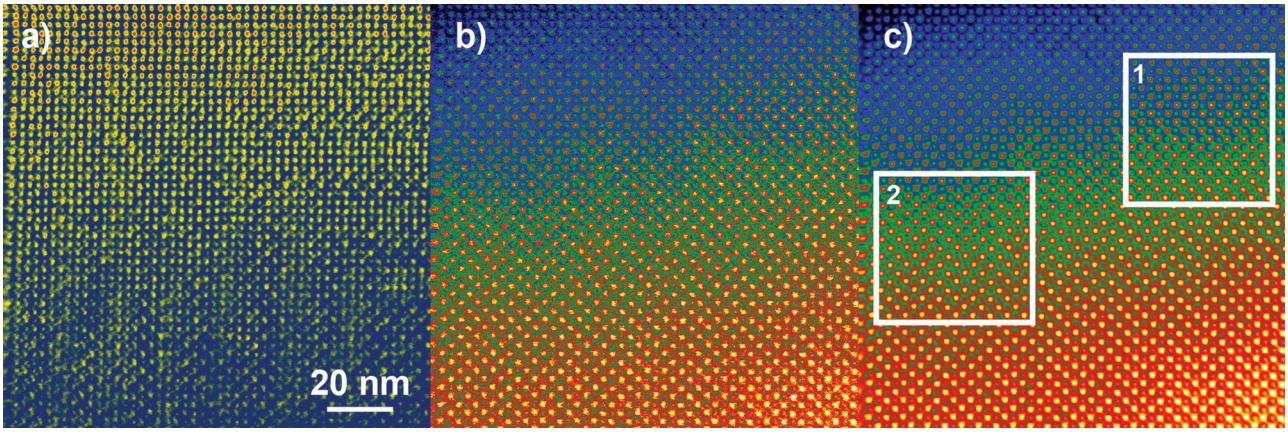

Figure 1. HRSTEM images of an area of the PLZT ceramic recorded along the [001] direction in an area containing a 90° domain boundary, all false coloured to enhance the contrast for the benefit of the reader: a) bright field image showing the stripes associated with the layered structures; b) a single high angle annular dark field image; c) a sum image created by cross-correlating 28 scans of the same area in order to remove the effects of drift in the image recording and electronic noise in the individual acquisitions; two areas analysed in this paper are indicated by the boxes.

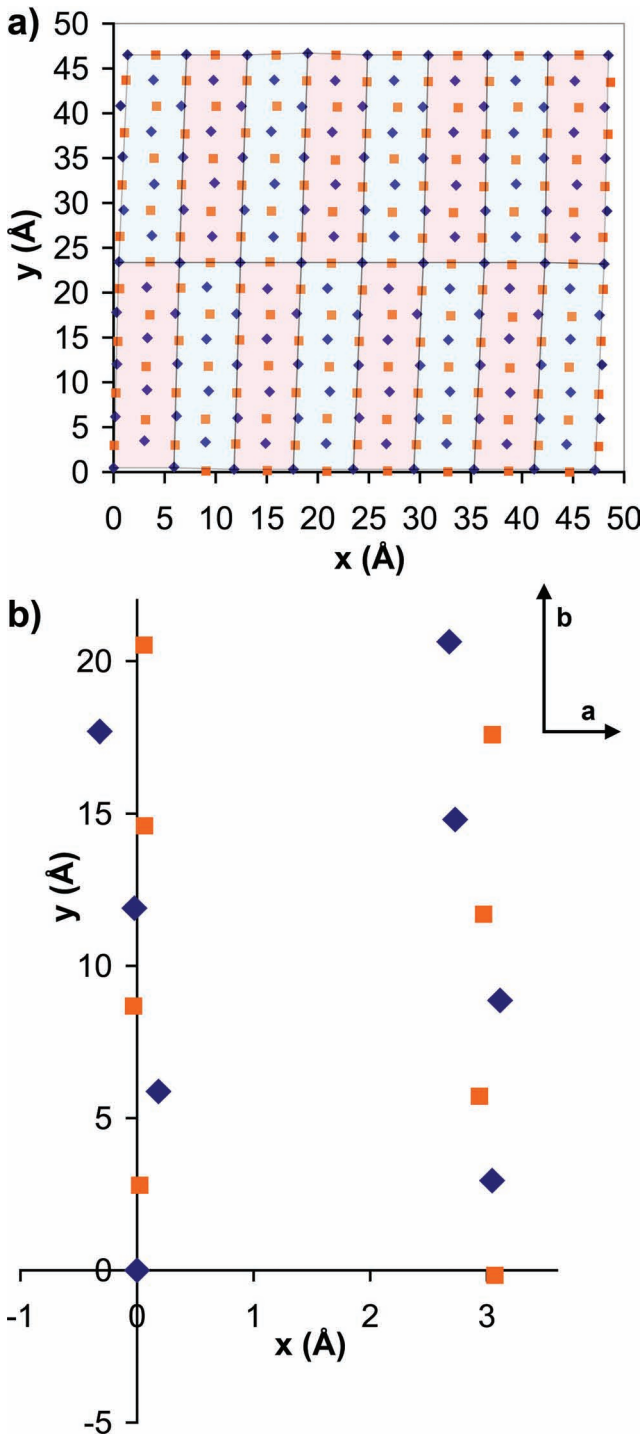

Figure 2. Graphs showing extracted cation positions from area 1 of the image shown in Figure 1c, blue diamonds are lead positions and orange squares are zirconium/titanium positions: a) raw positions showing the scan distortion in the initial image but already clearly showing a pattern of repeating unit cells; b) average after full distortion correction of 16 cells, showing a very clear repeating pattern of lead ion displacements in an orthorhombic cell, error bars are typically smaller than the data points and are not shown.

square along the [001] projection so simple linear transformations were applied to the measured peak positions to restore the squareness on average. Such corrections were rotation of the peak rows to horizontal, correction of the obvious shear in Figure 2a, correction of any difference between horizontal and vertical magnification, followed by some more local corrections (e.g., slight variations in horizontal magnification across the image). After correction, all identified cells could be zero shifted and overlaid to allow comparison and averaging of atomic positions. This resulted in an extremely good agreement between all sixteen unit cells in the area shown in Figure 2a and the average position for each atom column is plotted in Figure 2b. The pattern of ionic displacements across the unit cell is clearly seen in Figure 2b: the Pb ions are displaced to the right in the lower half of the unit cell and to the left in the upper half of the cell. Meanwhile, the Zr/Ti ions hardly move at all across the cell. Please note that although it would be ideal to plot error bars on this graph to show the very small uncertainties in the measurements, for most columns the error bars would be so short as to be impossible to see. Lead columns are always located with a standard deviation of better than 10 pm and show an average standard deviation of 6 pm. The more weakly scattering Zr/Ti columns cannot be located quite as accurately due to some peaks being affected by the tails of the strong Pb peaks but the average standard deviation was still 9 pm. This precision of around or better than 10 pm is an exceptionally good result for HRSTEM and approaches the accuracy of atom site location in recent HRTEM studies.[12]

A representative area of vertical stripes from the left hand side (area 2) of Figure 1c was also processed in a similar manner and averaged atomic column positions are plotted in **Figure 3**. In this case, the repeat happens every six layers in the *x*-direction and is characterised by a pattern of three layers with lead displaced downwards (i.e., the negative *y*-direction) followed by three layers with lead displaced upwards. As before, the Zr/Ti ions move very little across the cell. As for the 8-layer structure plotted in Figure 2b, the precision of atom site location is exceptional with an average for lead sites of 6 pm and for zirconium/titanium sites of 7 pm.

3. Discussion

In the best known antiferroelectric, $PbZrO_3$, the antiferroelectric ordering manifests itself as an antiparallel shift of Pb columns

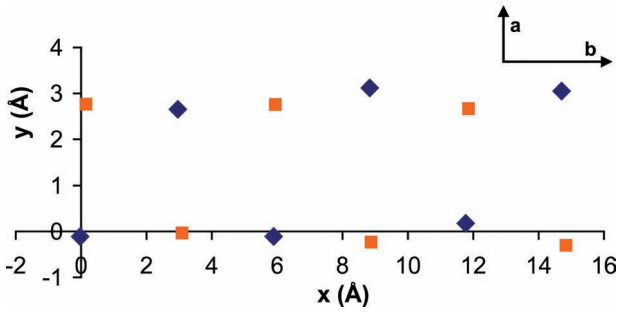

Figure 3. Atomic positions extracted from processing 21 unit cells from area 2 of the image in Figure 1c after full correction for all scan distortions, blue diamonds are lead positions and orange squares are zirconium/titanium positions. Most error bars are smaller than the marked data points and are consequently not shown.

in a 4-layer stacking along the *b*-direction of the orthorhombic unit cell with half the unit cell having Pb ions shifted in one direction by about 28 pm and the other half shifted in the opposite direction by the same amount. In conjunction with this shift of Pb atoms, additionally the O atoms shift in the opposite direction to the Pb atoms whereas the Zr atoms are hardly shifted. This may be seen in the schematic diagram of the structure in a [001] projection shown in **Figure 4**a, for the published structure of Corker et al.[25] The shifts of the lead ions are plotted against position along the *b* axis in Figure 4b for this published structure to provide a comparison to the experimental results of the present study. Shifts of the Pb ions against position along the *b* axis is shown in Figure 4c for the 8-layer structure of Figure 2b and in Figure 4d for the 6-layer structure of Figure 3. Both of these structures show a key similarity to the antiferroelectric $PbZrO_3$ in that in all cases the unit cell clearly splits into two halves with Pb ions shifted in opposite directions in each half of the cell; this demonstrates unambiguously that these different stacking sequences found in the incommensurate phase are antiferroelectric. Additionally, peak displacements in both the 6- and 8-layer cells approach the 28 pm seen for $PbZrO_3$ with 27 ± 8 pm for the 8-layer structure and 28 ± 4 pm for the 6-layer structure; this excellent match between displacements measured from HRSTEM and those measured previously using X-ray diffraction gives us great confidence in the quality of measurement that is possible using quantification of HRSTEM images. It should also be noted that little in the way of strong modulations is found in the Zr/Ti peak positions, which is the same tendency as for the commensurate $PbZrO_3$ phase. Nevertheless, one significant difference from the refined $PbZrO_3$ structure is evident in these 6- and 8-layer stackings, which is that the displacement of the lead ions from the positions they would have adopted in a cubic structure shows a near-sinusoidal dependence on position in the unit cell; and a sinusoidal fit to the lead ion shifts is plotted in Figure 4c and 4d. Clearly, the polarisation is not constant in the two halves of the unit cell and some Pb ions are hardly shifted in the 8-layer structure.

Previous studies have used atomic shifts measured using HRTEM[26–28] and HRSTEM to interpret the local polarisation in a ferroelectric and in a similar manner, we calculate the local polarisation for each plane of Pb atoms perpendicular to the unit cell, since for any of these antiferroelectrics, polarisation will arise at the atomic scale in stripes perpendicular to the *b* axis. It is possible to calculate the polarisation in each stripe in the $PbZrO_3$ structure using the standard definition of polarisation:

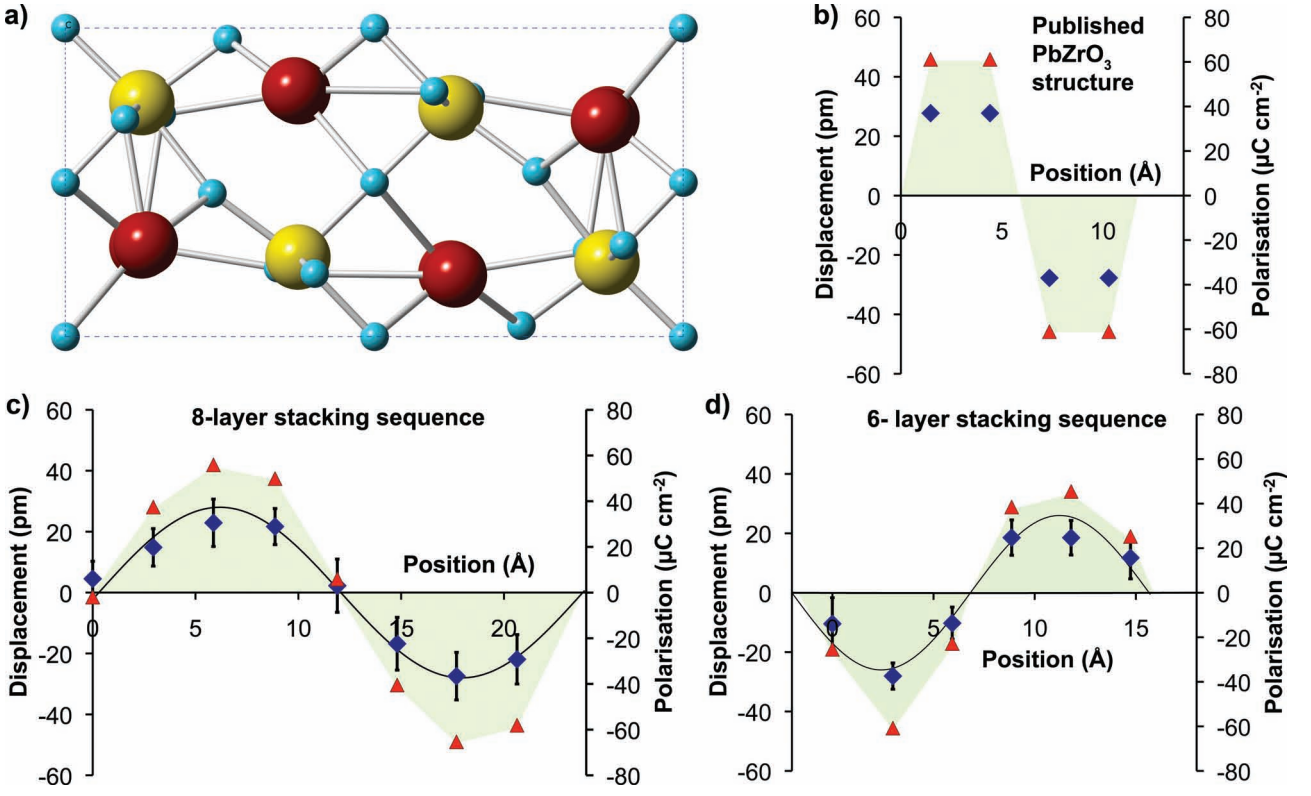

Figure 4. Comparison of the structure of $PbZrO_3$ to the 6- and 8-layer stacking sequences found in the incommensurate phase: a) Schematic diagram of the unit cell of the $PbZrO_3$ structure viewed along the [001] direction; Pb ions are marked in red, Zr ions in yellow, and O ions in cyan. Atomic positions used were those of Corker et al.[25] Note that in the left hand half of the cell Pb ions are shifted upwards and O downwards with respect to the almost stationary Zr ions, whereas in the right hand half the Pb ions are shifted downwards and the O ions upwards; b–d) Displacements of lead atoms perpendicular to the long b axis of the unit cell as a function of distance along this long axis (blue diamonds, left hand *y*-axis) together with calculated polarisation (red triangles and green shading–right hand *y*-axis); b) $PbZrO_3$ as refined by Corker et al.,[25] c) 8-layer unit cell shown in Figure 2b with sinusoidal fit superimposed; d) 6-layer unit cell shown in Figure 3 with a sinusoidal fit superimposed.

$$P_S = \frac{1}{V}\sum \delta_i Z_i \quad (1)$$

where V is the volume of the box of atoms under consideration, δ_i is the displacement of atom i, and Z_i is the charge of atom i. This was done using Born effective potentials for $PbZrO_3$[29] of $Z^*_{Pb} = 3.93$, $Z^*_{Zr} = 5.89$, $Z^*_{O\perp} = -2.5$, and $Z^*_{O\parallel} = -4.82$, as has been previously used for polarisation estimation from HRTEM[27] and HRSTEM[19] images of ferroelectrics; atomic position data for $PbZrO_3$ was taken from Corker et al.[25] In this structure (shown in Figure 4) oxygen moves antiparallel to lead atoms with very small shifts of the zirconium/titanium atoms meaning that the main contributions to the polarisation come from the oxygen and lead shifts. The calculated polarisation against position along the b axis for $PbZrO_3$ is plotted in Figure 4b. In the present work, only HAADF images were used, which do not reveal oxygen positions, and oxygen shifts were calculated on the assumption that these are similar to those in X-ray structure refinements of $PbZrO_3$. Since, this experimental work was carried out, the imaging and quantification of oxygen positions in bright field[16] and annular bright field images[30] has been achieved, and such techniques would be a valuable addition to the present kind of studies in the future allowing direction quantification of oxygen shifts and octahedral tilts. Nevertheless, assuming $PbZrO_3$-like oxygen shifts in the 8- and 6-layer structures and calculating polarisation as for $PbZrO_3$ above, polarisation was plotted against position in Figure 4c and d. These polarisation values peaking in the range ~60 μC cm^{-2} are quite comparable to those calculated for the $PbZrO_3$ structure and of a similar magnitude than those calculated from HRTEM images of Ti-rich, highly tetragonal PZT[27] (~80 μC cm^{-2}). Thus, it is clearly demonstrated that HRSTEM-based methods can provide a valuable complement to HRTEM for the measurement of polarisation at the nanoscale in phases with permanent polarisation.

The elucidation of the details of the cation stackings in the incommensurate antiferroelectric phase of lanthanum-doped PZT is highly significant in understanding this phase and its relationship to its neighbouring phases: the commensurate 4-layer antiferroelectric phase typified by $PbZrO_3$, and the ferroelectric rhombohedral phase found in PZT with Zr:Ti < 0.96. Previous observations using HRTEM have suggested possible 8- and 7-layer orderings and it was suggested by He and Tan[9] that the 8-layer structure might consist of four layers with the polarisation along the positive **a** direction followed by four layers with a polarisation antiparallel to this, but up until now it has been impossible to prove such speculations. This present work shows that the model of He and Tan[9] is broadly correct although the antiferroelectric modulation appears to have a more sinusoidal form. It is not currently clear why the area observed had a 6-layer stacking preferred to one side of a 90° domain boundary and an 8-layer stacking on the other, but similar stackings have been observed in other specimens, and it is clear that this was not just a thickness or specimen preparation effect, but a real part of the bulk structure. One thing that is clear for both the 6- and 8-layer stackings is that the stripes of polarisation with the same sign are significantly wider than in the commensurate $PbZrO_3$ structure and this is a strong indication that the preference for an antiferroelectric ordering is somewhat weaker in this La-doped compositions than in the pure $PbZrO_3$ composition. In other words, the incommensurate antiferroelectric phase is a compromise between antiferroelectric and ferroelectric orderings where the overall ordering is antiferroelectric but locally relatively wide stripes (up to >1 nm) have the same polarisation and are thus locally ferroelectric.

This work demonstrates that quantitative STEM techniques are of great value in understanding the detailed atomic orderings in one complex structure with only nanometre scale ordering at a morphotropic phase boundary between ferroelectric and antiferroelectric phases. It is well known that other morphotropic boundaries between two different ferroelectric phases also result in highly complex nanodomain structures, e.g., in $Pb(Zr,Ti)O_3$[31] or in $Pb(Mn,Nb)O_3$-$PbTiO_3$.[32] It is, therefore, to be expected that similar quantitative STEM approaches will yield more detailed information about local atomic orderings in such nanostructures, in a way that would never be accessible by broad beam diffraction techniques.

4. Conclusions

It has been shown that the incommensurate phase found at the phase boundary between ferroelectric and antiferroelectric orderings in lanthanum-doped, zirconium-rich lead zirconate titanate is composed of 6- and 8-layer stacking sequences. Both sequences have had their cation structures determined by quantitative atom position measurement from high angle annular dark field images recorded at the SuperSTEM facility. This revealed a near-sinusoidal modulation of Pb-ion positions across both stacking sequences and a clearly antiferroelectric ordering. The peak values of Pb displacement in both the 6- and 8-layer orderings of 27 and 28 pm match well to published values for $PbZrO_3$ of 28 pm. These ion positions were used to estimate the local polarisation variation across each structural unit assuming similar oxygen displacements to those in $PbZrO_3$ giving peak values of about 60 μC cm^{-2}, which is also very similar to peak values in $PbZrO_3$. The unambiguous demomstration that the polarisation stripes in the incommensurate antiferroelectric phase of lanthanum-doped lead zirconate titanate are wider than in the well-known $PbZrO_3$ antiferroelectric structure demonstrates that this incommensurate phase represents a bridging phase between antiferroelectric and ferroelectric polarisation orderings in the lead zirconate titanate system.

5. Experimental Section

Ceramics were made according to the stoichiometry of $(Pb_{0.96}La_{0.04})(Zr_{0.9}Ti_{0.1})_{0.99}O_3$ from oxide powders by a conventional method of milling, calcination at 800 °C for 1 h, grinding, cold uniaxial pressing into discs, and sintering at 1250 °C for 1 h in a covered platinum crucible, as described in more detail elsewhere.[11] Samples for transmission electron microscopy were then prepared by sawing thin slices, polishing to ~120 μm thickness, dimpling, and argon ion milling at 4 kV followed by final milling at 500 eV to remove surface damage, and coated with a few nm of carbon to minimise charging under the electron beam.

Scanning transmission electron microscopy was carried out using the NION UltraSTEM microscope (Kirkland, WA, USA) at the SuperSTEM laboratory operated at an accelerating voltage of 100 kV and probe semiangle of 36 mrad and the images analysed in this work were

collected using the HAADF mode using a detector with inner radius of 101 mrad and an effective outer radius of 185 mrad. To reduce the effect of scan distortions and readout noise, multiple images were recorded from each area and then cross correlated and summed to produce a sum image using the "SDSD drift correction" plugin[24] for Digital Micrograph (Gatan Inc., Pleasanton, CA). Quantitative measurements of peak positions in images with sub-pixel precision were made using iMtools software.[33] It should be noted that the thinnest regions of the images containing the structures of interest were used for the quantitative measurements, although it was apparent from inspection of the images that very similar structures were apparent all the way into the thicker regions of the images. Measurement of image distortions was performed using Microsoft Excel on spreadsheets of extracted peak positions; least squares fitting was used to find the gradients of straight lines of peaks, and corrections to the positions to account for scan distortions were then performed by simple linear mathematics. Further details of image processing and data analysis procedures are provided in the Supporting Information.

Supporting Information

Supporting Information is available from the Wiley Online Library or from the author.

Acknowledgements

The support of the EPSRC for the SuperSTEM facility is gratefully acknowledged. The work on data analysis with L.H. was made possible by the provision of grants from the EPSRC (EP/H028218/1) and the Alexander von Humboldt foundation to I.M. to cover the costs of a visit to the Forschungszentrum Jülich, together with support from the DFG for the Ernst Ruska Centre. A.P.-B. thanks the Royal Society of London for short-term visitor (2007) and international travel (2008) awards, and to the ICTP (Trieste-Italy) for financial support of Latin-American Network of Ferroelectric Materials (NET-43). R.V. acknowledges the support of the CONACYT for the provision of a PhD studentship.

Received: May 27, 2011
Revised: September 29, 2011
Published online: November 8, 2011

[1] D. Damjanovic, *Appl. Phys. Lett.* **2010**, *97*, 062906.
[2] I. M. Reaney, D. I. Woodward, C. Randall, *J. Am. Ceram. Soc.* **2011**, *94*, 2242.
[3] Y. J. Chang, J. Y. Lian, Y. L. Wang, *Appl. Phys. A-Mater. Sci. Process.* **1985**, *36*, 221.
[4] J. S. Speck, M. De Graef, A. P. Wilkinson, A. K. Cheetham, D. R. Clarke, *J. Appl. Phys.* **1993**, *73*, 7261.
[5] D. Viehland, D. Forst, J. F. Li, *J. Appl. Phys.* **1994**, *75*, 4137.
[6] Y. Cai, F. Phillipp, A. Zimmermann, L. Zhou, F. Aldinger, A. Ruhle, *Acta Mater.* **2003**, *51*, 6429.
[7] J. Knudsen, D. I. Woodward, I. M. Reaney, *J. Mater. Res.* **2003**, *18*, 262.
[8] T. Asada, Y. Koyama, *Phys. Rev. B* **2004**, *70*, 104105.
[9] H. He, X. Tan, *Phys. Rev. B* **2005**, *72*, 024102.
[10] I. MacLaren, R. Villaurrutia, A. Peláiz-Barranco, *J. Appl. Phys.* **2010**, *108*, 034109.
[11] A. Peláiz-Barranco, J. D. S. Guerra, O. Garcia-Zaldivar, F. Calderon-Pinar, E. B. Araujo, D. A. Hall, M. E. Mendoza, J. A. Eiras, *J. Mater. Sci.* **2008**, *43*, 6087.
[12] L. Houben, A. Thust, K. Urban, *Ultramicroscopy* **2006**, *106*, 200.
[13] K. W. Urban, *Nat. Mater.* **2009**, *8*, 260.
[14] C. L. Jia, M. Lentzen, K. Urban, *Science* **2003**, *299*, 870.
[15] R. J. Zeches, M. D. Rossell, J. X. Zhang, A. J. Hatt, Q. He, C. H. Yang, A. Kumar, C. H. Wang, A. Melville, C. Adamo, G. Sheng, Y. H. Chu, J. F. Ihlefeld, R. Erni, C. Ederer, V. Gopalan, L. Q. Chen, D. G. Schlom, N. A. Spaldin, L. W. Martin, R. Ramesh, *Science* **2009**, *326*, 977.
[16] A. Y. Borisevich, H. J. Chang, M. Huijben, M. P. Oxley, S. Okamoto, M. K. Niranjan, J. D. Burton, E. Y. Tsymbal, Y. H. Chu, P. Yu, R. Ramesh, S. V. Kalinin, S. J. Pennycook, *Phys. Rev. Lett.* **2010**, *105*.
[17] M. F. Chisholm, W. D. Luo, M. P. Oxley, S. T. Pantelides, H. N. Lee, *Phys. Rev. Lett.* **2010**, *105*.
[18] H. J. Chang, S. V. Kalinin, A. N. Morozovska, M. Huijben, Y. H. Chu, P. Yu, R. Ramesh, E. A. Eliseev, G. S. Svechnikov, S. J. Pennycook, A. Y. Borisevich, *Adv. Mater.* **2011**, *23*, 2474.
[19] C. T. Nelson, B. Winchester, Y. Zhang, S. J. Kim, A. Melville, C. Adamo, C. M. Folkman, S. H. Baek, C. B. Eom, D. G. Schlom, L. Q. Chen, X. Q. Pan, *Nano Lett.* **2011**, *11*, 828.
[20] A. Recnik, G. Möbus, S. Sturm, *Ultramicroscopy* **2005**, *103*, 285.
[21] A. M. Sanchez, P. L. Galindo, S. Kret, M. Falke, R. Beanland, P. J. Goodhew, *J. Microsc.-Oxf.* **2006**, *221*, 1.
[22] W. D. Pyrz, D. A. Blom, T. Vogt, D. J. Buttrey, *Angew. Chem. Int. Ed.* **2008**, *47*, 2788.
[23] X. H. Sang, K. Du, M. J. Zhuo, H. Q. Ye, *Micron* **2009**, *40*, 247.
[24] B. Schaffer, W. Grogger, G. Kothleitner, *Ultramicroscopy* **2004**, *102*, 27.
[25] D. L. Corker, A. M. Glazer, J. Dec, K. Roleder, R. W. Whatmore, *Acta Crystallogr. Sect. B-Struct. Commun.* **1997**, *53*, 135.
[26] C. L. Jia, V. Nagarajan, J. Q. He, L. Houben, T. Zhao, R. Ramesh, K. Urban, R. Waser, *Nat. Mater.* **2007**, *6*, 64.
[27] C. L. Jia, S. B. Mi, K. Urban, I. Vrejoiu, M. Alexe, D. Hesse, *Nat. Mater.* **2008**, *7*, 57.
[28] C. L. Jia, K. W. Urban, M. Alexe, D. Hesse, I. Vrejoiu, *Science* **2011**, *331*, 1420.
[29] P. Ghosez, E. Cockayne, U. V. Waghmare, K. M. Rabe, *Phys. Rev. B* **1999**, *60*, 836.
[30] S. D. Findlay, N. Shibata, H. Sawada, E. Okunishi, Y. Kondo, Y. Ikuhara, *Ultramicroscopy* **2010**, *110*, 903.
[31] L. A. Schmitt, K. A. Schonau, R. Theissmann, H. Fuess, H. Kungl, M. J. Hoffmann, *J. Appl. Phys.* **2007**, *101*.
[32] H. Wang, J. Zhu, X. W. Zhang, Y. X. Tang, H. S. Luo, *Appl. Phys. Lett.* **2008**, *92*.
[33] L. Houben, iMtools imaging processing software, http://www.er-c.org/methods/software.htm.